Nonreciprocal Wave Propagation in Multilayer Semiconductor Films at Frequencies Up to 200 GHz

Vee H. Mok, *Member, IEEE,* and Lionel E. Davis, *Life Fellow, IEEE*

***Abstract*—Three multilayer gyrotropic thin-film semiconductor waveguides comprising S-I GaAs/AlAs/n–GaAs/AlGaAs in a static magnetic field of 0.15 T have been analyzed over the frequency range of 0–200 GHz. The dispersion diagrams and field distributions show nonreciprocal propagation, and forward waves and backward waves depending on the order in which the films are stacked. Potential applications such as miniature phase shifters and isolators in the frequency range of 50–100 GHz with lengths of the order of micrometers are briefly discussed.**

***Index Terms*—Dispersion diagram, isolator, magnetoplasmon, nonreciprocal, phase shifter, semiconductors, thin films.**

I. Introduction

WAVEGUIDES containing gyrotropic materials, in particular, magnetized ferrites, have led to the realization of isolators, circulators, and phase shifters [1], [2]. The propagation of magnetostatic surface waves (MSSWs) on a ferrite/dielectric interface has been reviewed in a number of papers and books [3]–[6]. A thin-film isolator and multiport devices have recently been discussed [7], [8]. Also, a novel nonreciprocal ferrite image guide by Akyol and Davis [9], [10] has demonstrated nonreciprocal leaky-wave behavior. Electromagnetic surface waves on an interface between nonmagnetic media are well known [11] and their existence requires that one of the two dielectric constants is negative. A classical example is the support of optical plasmons on the interface between air and silver [12]. Surface-wave behavior along a single gyroelectric or isotropic semiconductor interface has been extensively investigated analytically and experimentally [13]–[18], and the references therein]. In 1972, Chiu and Quinn [13] analyzed magneto-plasma surface waves (i.e., magnetoplasmons or polaritons) for the three primary orientations of $\mathbf{B}_o$, i.e.: 1) $(\mathbf{B}_o \,||\, \mathbf{n}) \perp \mathbf{k}$; 2) $(\mathbf{B}_o \,||\, \mathbf{k}) \perp \mathbf{n}$; and 3) $\mathbf{B}_o \perp \mathbf{n} \perp \mathbf{k}$, where $\mathbf{n}$ is the normal to the surface and $\mathbf{k}$ is the direction of propagation. Brion and Wallis [14] found a branch of the dispersion curve not identified in [13] by considering a wider range of values of limiting relative permittivity (ε_∞). Marschall and Fischer [15] analyzed far infrared (FIR) polaritons on GaP thin films with $B_o = 0$. Hartstein and Burstein [16] reported experimental observation of nonreciprocal dispersion of FIR polaritons on an InSb/air interface and they obtained qualitative agreement with theory. They also discussed the possible effects of surface defects. In 1974, Wallis *et al.* [17] extended their earlier analysis [14] to discuss more general cases. In 1987, Kushwaha and Halevi [18] discussed the theoretical splitting of the dispersion curves due to resonance in a magnetoplasma transition layer using a InSb film on an MgO substrate as an example. The design and construction of isolators, circulators, and reflection beam isolators in the millimetric and submillimetric regions using the properties of magnetoplasmons in semiconductors have been reported by several authors [19]–[22]. Also, the nonreciprocal behavior of a grounded dielectric slab with a gyroelectric semiconductor layer as a superstrate, and the inverted structure, has also been reported [23].

In this paper, waveguiding on thin-film multilayer semiconductor structures is described in order to begin to explore the possible integration of miniature phase shifters and isolators on monolithic microwave integrated circuits (MMICs). Fabrication constraints are taken into account and three structures consisting of two or three submicrometer layers on a semiconductor substrate are studied for the first time. Nonreciprocal wave behavior is discussed in the frequency range of 50–200 GHz, where magnetoplasmon wavelengths are of the order of micrometers, i.e., two orders of magnitude smaller than many conventional passive devices in this frequency range. The structures comprise a semi-insulating (S-I) gallium arsenide (GaAs) substrate, undoped (U/D) aluminum arsenide (AlAs) buffer layer, U/D aluminum gallium arsenide (AlGaAs) layer, and a gyrotropic layer of high-quality n-type GaAs [24]. All the films are assumed lossless. A uniform external magnetic flux density (B_o) is applied parallel to the film surface and perpendicular to the direction of propagation. Dispersion diagrams (β versus f), together with field distributions for the transverse microwave magnetic field, are presented for the forward- and reverse-wave behavior for all three structures.

II. Theory

The S-I substrate and films are treated as lossless dielectrics. The gyroelectric n-GaAs film is modeled using the Drude–Zener model [25]–[27] assuming the electron collision

Manuscript received April 17, 2003.

The authors are with the Electromagnetics Centre for Microwave and Millimetre-Wave Design and Applications, Department of Electrical Engineering and Electronics, University of Manchester Institute of Science and Technology, Manchester M60 1QD, U.K. (e-mail: jimmymok@ieee.org; l.davis@umist.ac.uk).

Digital Object Identifier 10.1109/TMTT.2003.820167

frequency $\nu_c = 0$. In the presence of a mutually perpendicular static magnetic bias field and a sinusoidal electric field ($Ee^{j\omega t}$), the cyclotron motion of the mobile electrons causes gyroelectric behavior and the relatively massive holes are assumed to be stationary. Under these circumstances, and with the bias field in the $+y$-direction, the tensor relative permittivity $[\varepsilon]$ can be written in the form

$$[\varepsilon] = \begin{bmatrix} \xi & 0 & -j\eta \\ 0 & \zeta & 0 \\ +j\eta & 0 & \xi \end{bmatrix} \tag{1}$$

$$\xi = \varepsilon_r \left[1 - \frac{\omega_p^2}{(\omega - \omega_c^2)}\right] \tag{2}$$

$$\eta = \varepsilon_r \left[\frac{\omega_p^2 \omega_c}{\omega(\omega^2 - \omega_c^2)}\right] \tag{3}$$

$$\zeta = \varepsilon_r \left[1 - \frac{\omega_p^2}{\omega^2}\right]. \tag{4}$$

The term ε_r is the (isotropic) relative permittivity of the semiconductor magnetoplasma when $\omega_p = 0$ or $\omega/\omega_p \gg 1$ and $\omega/\omega_c \gg 1$. The symbol ω_p denotes the plasma frequency, and ω_c is the cyclotron frequency, defined by (5) and (6) respectively, as follows:

$$\omega_p = \sqrt{\frac{e^2 N_e}{\varepsilon_o \varepsilon_r m_e^*}} \tag{5}$$

$$\omega_c = \frac{e}{m_e^*} B_o \tag{6}$$

where ε_o is the permittivity of free space, e is the electron charge, m_e^* is the electron effective mass, N_e is the electron concentration, and B_o is the applied static magnetic field. The key criterion for the semiconductor to exhibit plasma behavior is $\omega_c > \nu_c$, where the collision frequency $\nu_c = e/m_e^* \mu_e$. For GaAs at 77 K, $m_e^* = 0.067 m_o$ kg [28], where m_o is the electron mass in vacuum having a value of 9.109×10^{-31} kg. With an electron mobility $\mu_e = 21\ m^2 V^{-1} s^{-1}$, the calculated collision frequency is $\nu_c = 0.12 \times 10^{12}\ s^{-1}$. With an applied magnetic flux density of $B_o = 0.15$ T, the cyclotron frequency is $\omega_c = 0.39 \times 10^{12}$ rad/s and the ratio $\omega_c/\nu_c = 3.15$. Hence, this combination of parameters satisfies the condition that $\omega_c > \nu_c$. The relative effective permittivity ε_{eff} experienced by the extraordinary (TM) wave in an unbounded semiconductor plasma is defined in (7) as follows:

$$\varepsilon_{\text{eff}} = \frac{\xi^2 - \eta^2}{\xi}. \tag{7}$$

The frequency dependence of ε_{eff} is shown in Fig. 1 for the parameters given above and frequency ranges of potential interest are defined. A singularity occurs at frequency f_{res} and this is referred to as the extraordinary wave resonance frequency. The frequencies f_A, f_{res}, and f_B indicated in Fig. 1 are defined in [27] and, at f_A and f_B, the magnitude of the gyrotropic ratio $\gamma = \eta/\xi$ is equal to unity. With the parameters defined above,

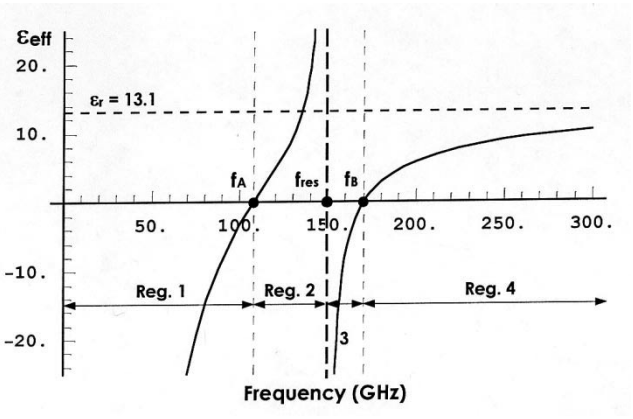

Fig. 1. Effective relative permittivity as a function of frequency for n-GaAs at liquid-nitrogen temperature (77 K) with a transverse magnetic flux density $B_o = 0.15$ T and TM mode propagation. The material is assumed to be lossless. $\varepsilon_r = 13.1, \omega_p = 0.85 \times 10^{12}$ rad/s and $\omega_c = 0.39 \times 10^{12}$ rad/s. $f_A = 107.79$ GHz, $f_{\text{res}} = 149.33$ GHz, and $f_B = 170.45$ GHz.

$f_A = 107.79$ GHz, $f_{\text{res}} = 149.33$ GHz, and $f_B = 170.45$ GHz. The effective relative permittivity is negative in two frequency regions, i.e., for $0 < f < f_A$ (region 1) and $f_{\text{res}} < f < f_B$ (region 3) and is positive for $f_A < f < f_{\text{res}}$ (region 2) and $f > f_B$ (region 4).

III. Semiconductor Multilayer Waveguide Structures

A. Design Constraints on a Multilayer Structure

In the fabrication of multilayer thin-film semiconductor structures, a lattice mismatch at the interface between differing materials causes stress that imposes constraints on the maximum allowable thickness of each film before dislocation causes film defects. Two important parameters in growing multilayer III–V semiconductor structures are strain and critical thickness and the relevant formulas are as follows [29], [30]:

$$\text{strain} = \frac{a_{\text{sup}} - a_{\text{sub}}}{a_{\text{sub}}} \tag{8}$$

$$\text{critical thickness} \approx \frac{a_{\text{sub}}}{2 \times \text{strain}} \tag{9}$$

where a_{sub} and a_{sup} are the values of lattice constant of the III–V semiconductors comprising the substrate and superstrate layer, respectively. If $a_{\text{sup}} > a_{\text{sub}}$, compressive (i.e., positive) strain occurs and the crystal structure of the superstrate layer compresses itself in order to match the size of the crystal structure of the substrate layer. In the reverse case, i.e., when $a_{\text{sup}} < a_{\text{sub}}$, a tensile (negative) strain occurs and the superstrate crystal structure relaxes in order to match the substrate crystal structure [31]. The critical thickness is the maximum permitted thickness of the layer before the crystal structure starts to dislocate itself in the system due to the strain (compressed or tensile). It is evident from (9) that the critical thickness is inversely proportional to the strain and it is necessary to take this point into consideration in the design of a multilayer waveguide. A general guide for growing high-quality multilayer structures by molecular beam

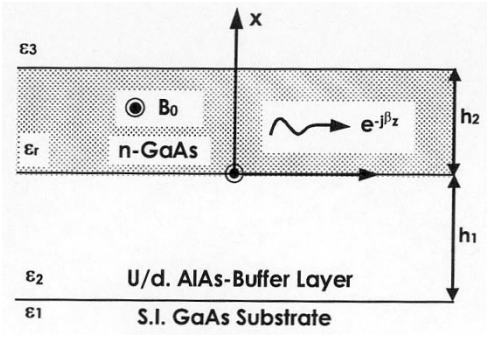

Fig. 2. Geometry of a two-film waveguide structure on a substrate.

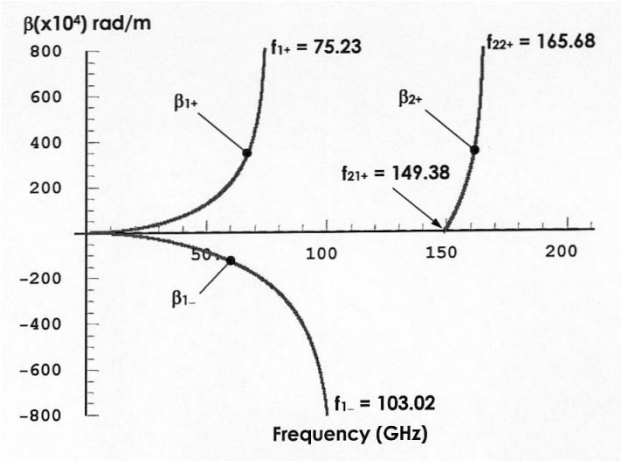

Fig. 3. Dispersion diagram of a two-film waveguide structure showing both forward and reverse propagation. S-I substrate: $\varepsilon_1 = 13.1$. U/D buffer layer: $\varepsilon_2 = 10.1, h_1 = 0.25$ μm. n-GaAs: $\varepsilon_r = 13.1, h_2 = 0.20$ μm. Air: $\varepsilon_3 = 1$. Applied magnetic flux density: $B_o = 0.15$ T.

epitaxy (MBE) is not to exceed a total structure thickness of 2–4 μm with a growth rate of 1 μm/h. These dimensions suggest that semiconductor films could be used as magnetoplasmon waveguides at millimetric wavelengths or bulk waveguides at terahertz and FIR wavelengths. This paper considers the properties of magnetoplasmons in these films.

B. Two-Film Waveguide

The four-region waveguide structure shown in Fig. 2 has two thin films. The structure consists of an S-I GaAs substrate, U/D AlAs buffer layer, a gyroelectric n-type GaAs layer, and air above. The buffer layer and the n-GaAs film have thicknesses $h_1 = 0.25$ μm and $h_2 = 0.2$ μm, and relative dielectric constants of $\varepsilon_2 = 10.1$ and $\varepsilon_r = 13.1$, respectively. The S-I GaAs substrate has $\varepsilon_1 = 13.1$ and the uppermost region is air with $\varepsilon_3 = 1$. The static magnetic flux density $\mathbf{B}_o$ is applied in the y-direction and propagation is in the z-direction $(e^{j(\omega t-\beta z)})$. For guiding to occur, the fields are evanescent in the substrate and air regions, with a transverse behavior described by $e^{k_1 x}$ and $e^{-k_3 x}$, respectively, where k_1 and k_3 are both positive real. Assuming TM modes (H_y, E_x, and E_z) and $\partial/\partial y = 0$, the magnetic field H_y for each of the four regions can be written as follows:

$$H_y = \begin{cases} A_1 e^{-k_3(x-h_2)}, & x \geq h_2 \\ A_2 e^{-k_r x} + A_3 e^{k_r x}, & 0 \leq x \leq h_2 \\ A_4 e^{-k_2 x} + A_5 e^{k_2 x}, & -h_1 \leq x \leq 0 \\ A_6 e^{k_1(x+h_1)}, & x \leq -h_1. \end{cases} \tag{10}$$

Phase-matching conditions yield

$$k_3 = \sqrt{\beta^2 - k_o^2} \tag{11}$$
$$k_2 = \sqrt{\beta^2 - \varepsilon_2 k_o^2} \tag{12}$$
$$k_r = \sqrt{\beta^2 - \varepsilon_{\text{eff}} k_o^2} \tag{13}$$
$$k_1 = \sqrt{\beta^2 - \varepsilon_1 k_o^2} \tag{14}$$

where $k_o^2 = \omega^2 \mu_o \varepsilon_o$ is the free-space propagation constant, β is the guided-wave phase constant, and ε_o and μ_o are the permittivity and permeability of a vacuum. The other field components (E_x and E_z) for the TM modes are obtained from Maxwell's equations for the respective regions as follows:

$$E_x = \begin{cases} \dfrac{\beta}{\omega \varepsilon_o \varepsilon_i} H_y, & \text{for } i = 1,2,3 \\ \dfrac{1}{\omega \varepsilon_o \varepsilon_{\text{eff}}} \left(\beta H_y + \gamma \dfrac{\partial H_y}{\partial x} \right), & \text{for } \varepsilon_r \end{cases} \tag{15}$$

$$E_z = \begin{cases} \dfrac{-j}{\omega \varepsilon_o \varepsilon_i} \cdot \dfrac{\partial H_y}{\partial x}, & \text{for } i = 1,2,3 \\ \dfrac{-j}{\omega \varepsilon_o \varepsilon_{\text{eff}}} \left(\gamma \beta H_y + \dfrac{\partial H_y}{\partial x} \right), & \text{for } \varepsilon_r. \end{cases} \tag{16}$$

The propagation constant β is obtained from the solution of the six homogeneous equations that result from solving the boundary conditions by matching the tangential components of H_y and E_z. In matrix notation, this leads to the following equation system:

$$CA = 0 \text{ where } \sum_{i=1}^{6} C_{ni} A_i = 0, \qquad n = 1,2,\ldots,6. \tag{17}$$

The homogeneous equation system has nontrivial solutions only when its system determinant $|C| = 0$. A program written in Mathematica 4.0 was used to obtain numerical solutions directly by searching for zeros of the unexpanded determinant. Once the propagation constant β value is found, one of the coefficients (A_{1-6}) is set to one and the remaining coefficients are found accordingly by solving the $CA = 0$ system.

Fig. 3 presents the dispersion diagram β versus f over a frequency range of 0–200 GHz. It can be seen that the first mode of the forward wave (β_{1+}) starts from $f = 0$ (Fig. 1, region 1), rises, and asymptotically approaches infinity at $f_{1+} = 75.23$ GHz, i.e., below f_A. The second mode of the forward wave (β_{2+}) which is associated with frequency region 3 (Fig. 1), starts from $f_{21+} = 149.38$ GHz, again rises, and

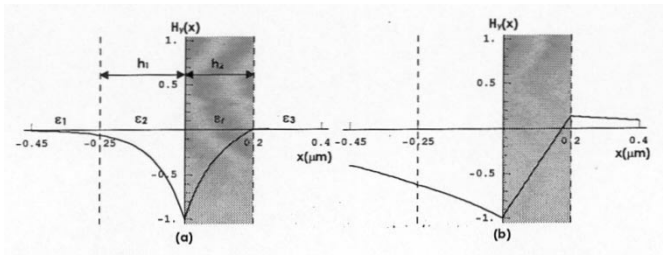

Fig. 4. $H_y(x)[t=0, z=0]$ at $f = 75$ GHz in region 1. (a) β_{1+}. (b) β_{1-}.

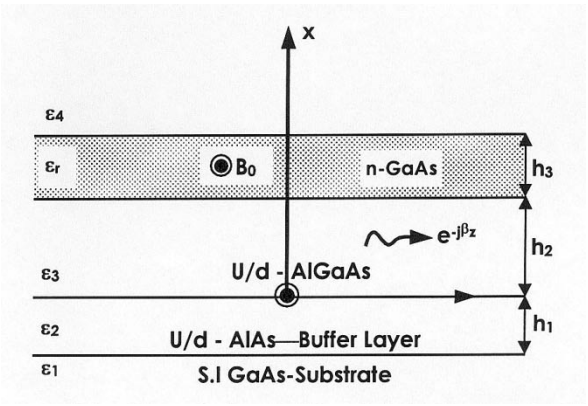

Fig. 5. Geometry of a three-film waveguide structure-type I.

asymptotically approaches infinity at $f_{22+} = 165.68$ GHz, i.e., below f_B. (It should be noted that, although it is not clear due to the scale of the graph, the β_{2+} branch starts at a point where $\beta_{2+} > 0$. The wave at such a point has been termed a "pseudosurface wave" [17] because the wave is not evanescent in both external media. This point is discussed in more detail in connection with the three-film structure later in this paper.) For the reverse propagation, β_{1-} starts from origin, rises, and asymptotically approaches infinity at frequency $f_{1-} = 103.02$ GHz, i.e., below f_A. A second reverse wave does not exist below 200 GHz.

The transverse variation of $H_y(x)[t=0, z=0]$ for the first forward and reverse waves at 75 GHz are shown in Fig. 4(a) and (b). The thicknesses of the U/D AlAs and n-GaAs films, i.e., $h_1 = 0.25$ μm and $h_2 = 0.2$ μm, are indicated by the vertical dashed lines. It can be seen that the field peaks at the n-GaAs/AlAs interface for both directions of propagation, but with the reverse wave, there is greater penetration into both the substrate and air regions. The field displacement from one side of the n-GaAs film to the other sometimes seen on reversal of the direction of propagation is suppressed by the highly asymmetric dielectric loading on each side of the n-GaAs film. For the second forward wave, over the range $f_{21+} < f < f_{22+}$ (Fig. 3), the field distribution is similar to that shown in Fig. 4(a).

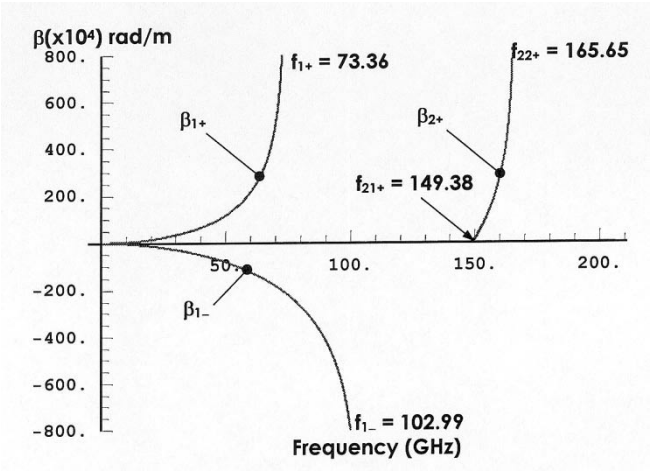

Fig. 6. Dispersion diagram of a three-film waveguide structure-type I showing both forward and reverse propagation. S-I substrate: $\varepsilon_1 = 13.1$. U/D buffer layer: $h_1 = 0.25$ μm, $\varepsilon_2 = 10.1$. U/D AlGaAs film: $h_2 = 1.0$ μm, $\varepsilon_3 = 11$. n-GaAs film: $h_3 = 0.2$ μm, $\varepsilon_r = 13.1$. Air: $\varepsilon_4 = 1$. $B_o = 0.15$ T.

C. Three-Film Waveguide Structure—Type I

The addition of a third film to the two-film structure enables the effect of asymmetry in the dielectric constant of the "cladding" external to the n-GaAs film to be studied. The dispersion diagram of the three-film waveguides depends upon the order in which the films are stacked, which is described below. The first of the two proposed three-film structures is shown in Fig. 5. It consists of an S-I GaAs substrate, U/D AlAs buffer layer, U/D AlGaAs layer, and a gyroelectric n-GaAs film with air above. The films have thicknesses $h_1 = 0.25$ μm, $h_2 = 1.0$ μm, and $h_3 = 0.2$ μm, respectively. The dielectric constant of U/D AlGaAs (ε_3) is 11. The n-GaAs film is uniformly magnetized in the y-direction and the wave is propagating in the z-direction. The transverse variation in the S-I GaAs substrate and air regions is given by $e^{k_1 x}$ and $e^{-k_4 x}$, respectively, and the transverse magnetic field H_y can be written as follows:

$$H_y = \begin{cases} A_1 e^{-k_4(x-h_2-h_3)}, & x \geq h_2+h_3 \\ A_2 e^{-k_r(x-h_2)} + A_3 e^{k_r(x-h_2)}, & h_2 \leq x \leq h_3 \\ A_4 e^{-k_3 x} + A_5 e^{k_3 x}, & 0 \leq x \leq h_2 \\ A_6 e^{-k_2 x} + A_7 e^{k_2 x}, & -h_1 \leq x \leq 0 \\ A_8 e^{k_1(x+h_1)}, & x \leq -h_1 \end{cases} \tag{18}$$

with

$$k_4 = \sqrt{\beta^2 - k_o^2}. \tag{19}$$

Solving the boundary conditions by matching the tangential components of H_y and E_z yields eight homogeneous equations, which can be represented by (17), where the coefficient is A_{1-8}. The dispersion diagram was obtained using the same procedure as before and is shown in Fig. 6. It can be seen that it is very similar to Fig. 3 for the two-film structure. It can be seen that increasing the dielectric constant beneath the n-GaAs film from

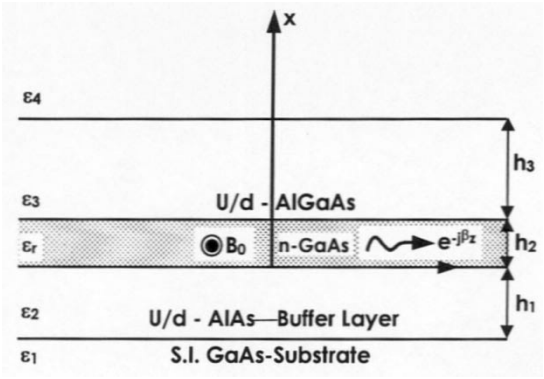

Fig. 7. Geometry of a three-film waveguide structure-type II.

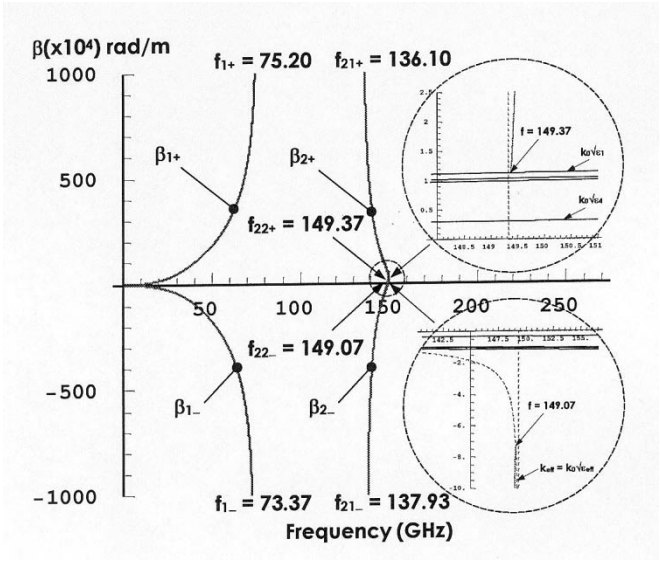

Fig. 8. Dispersion diagram of a three-film waveguide structure-type II showing both forward and reverse propagation. S-I GaAs substrate: $\varepsilon_1 = 13.1$. U/D AlAs buffer layer: $h_1 = 0.25\ \mu$m, $\varepsilon_2 = 10.1$. n-GaAs film: $h_3 = 0.2\ \mu$m, $\varepsilon_r = 13.1$. U/D AlGaAs film: $h_2 = 1.0\ \mu$m, $\varepsilon_3 = 11$. Air: $\varepsilon_4 = 1$. $B_o = 0.15$ T.

10.1 (U/D AlAs) to 11.0 (U/D AlGaAs) has left the second forward mode (β_{2+}) unaffected, but has slightly changed the first forward mode (β_{1+}). The asymptotic frequency f_{1+} is reduced by 1.87 GHz and the isolation bandwidth $\mathrm{B/W} = f_{1-} - f_{1+}$ has increased from 27.79 to 29.63 GHz. The distribution of $H_y(x)$ on each branch of the dispersion diagram is similar to the behavior shown in Fig. 4(a) and (b), except it is more tightly bound to the n-GaAs/AlGaAs (lower) interface. Graphs of the field distribution are omitted for brevity. Again, the field displacement with the reversal of the direction of propagation does not occur.

D. Three-Film Waveguide Structure—Type II

The geometry of the type-II three-film waveguide structure is shown in Fig. 7 and it is a rearrangement of the structure shown in Fig. 5. It consists of an S-I GaAs substrate, U/D AlAs buffer layer, a gyroelectric n-GaAs film, and an U/D AlGaAs film with air above. The individual film thicknesses are the same as before, i.e., $h_1 = 0.25\ \mu$m, $h_2 = 0.2\ \mu$m, and $h_3 = 1.0\ \mu$m. As with the previous structures, $\mathbf{B}_o$ is applied parallel to the film surface and perpendicular to the direction of propagation and the fields in the S-I GaAs substrate, and the air region are described by $e^{k_1 x}$ and $e^{-k_4 x}$. The magnetic field H_y for each of the five regions can be written in a similar form to (18), but with two layers interchanged.

The dispersion diagram can be obtained as before, using the boundary conditions on H_y and E_z and using (17). The result is shown in Fig. 8 and it has some significantly different features from Figs. 3 and 6. There are two branches for the reverse wave (β_{1-} and β_{2-}), whereas there was only one branch for the reverse wave in Figs. 3 and 6. The splitting in the asymptotic frequencies for β_{1+} and β_{1-}, $f_{1+} = 75.2$ GHz and $f_{1-} = 73.37$ GHz is less than was seen in Figs. 3 and 6. The H_y field distribution for the first forward and reverse waves at 70 GHz are shown in Fig. 9(a) and (b), respectively. For the first forward wave (β_{1+}), the magnetoplasmon is shown [see Fig. 9(a)] to be concentrated primarily at the n-GaAs/AlAs (lower) interface, whereas for the first reverse wave (β_{1-}), it is shown [see Fig. 9(b)] to be concentrated primarily at the n-GaAs/AlGaAs (upper) interface. Thus, nonreciprocal field displacement occurs depending on the direction of propagation because the asymmetry in the adjacent dielectric loading is not too large to prevent it. Unlike the first pair, the second pair of magnetoplasmons (β_{2+}, β_{2-}), associated with region 2 in Fig. 8, exhibit backward-wave behavior and their asymptotic frequencies (f_{21+}, f_{21-}) are very close together. The branches do not terminate at $\beta = 0$, and the β_{2-} end point is shown on a very enlarged scale in Fig. 10(b). Branch β_{3+} (not shown in Fig. 8) terminates on the line of $k_o\sqrt{\varepsilon_1}$ at 149.37 GHz. It can be seen from (14) and Fig. 10(a) that this condition implies that $k_1 = 0$, i.e., the field is no longer guided at the interface between the GaAs substrate and U/D AlAs (the "pseudosurface waves" condition [17]). Branches β_{2+} and β_{2-} terminate very close to $k_o\sqrt{\varepsilon_{\mathrm{eff}}}$ at 149.07 GHz and, in this case, the field is no longer guided at the interface between the n-GaAs and the U/D AlGaAs/air regions. Near the center of the band, at 140 GHz, the field distributions of $H_y(x)$ and $E_x(x)$ are as shown in Figs. 11(a) and (b) and 12(a) and (b) for the β_{2+} and β_{2-} branches, respectively. (Each of the graphs is normalized for clarity.) The distribution of the Poynting vector $\mathbf{P}_z(x) = \mathbf{E}_x \times \mathbf{H}_y$, computed from the unnormalized data, is shown in Fig. 13(a) and (b), but is presented here in normalized form. The backward-wave nature of these magnetoplasmons can be confirmed by integrating the Poynting vector over the range $-\infty < x < \infty$, i.e., the multilayer cross section. The Poynting vector is oppositely directed inside and outside the n-GaAs film, but it can be seen that the strong concentration of E_x and H_y within the n-GaAs film gives rise to the backward-wave behavior. On β_{2+}, the power density is concentrated nearer the n-GaAs/AlGaAs (upper) interface and, on β_{2-}, the concentration is more towards the n-GaAs/AlAs (lower) interface. As a result, as the frequency is decreased and β_{3+} approaches cutoff, the field concentration on both branches tends more towards the lower n-GaAs interface.

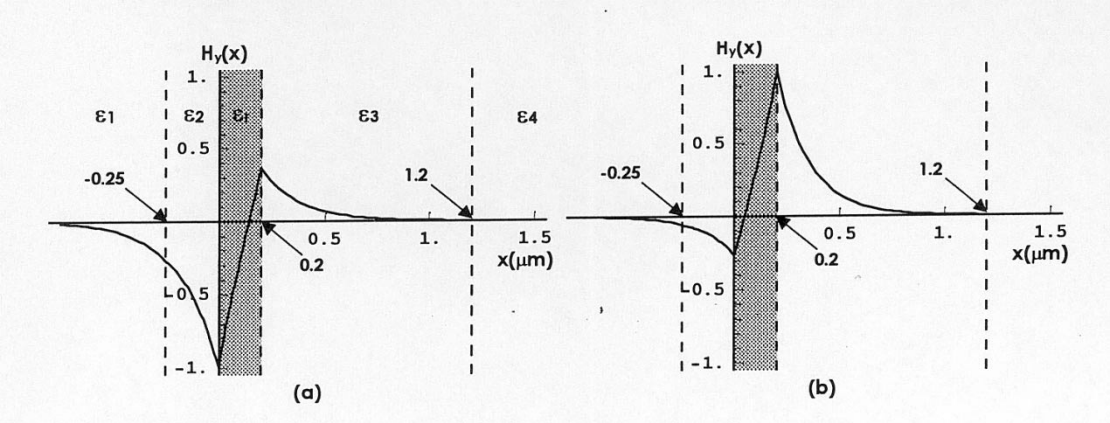

Fig. 9. $H_y(x)[t=0, z=0]$ at $f = 70$ GHz in region 1. (a) β_{1+} branch. (b) β_{1-} branch. (Field components in normalized units.)

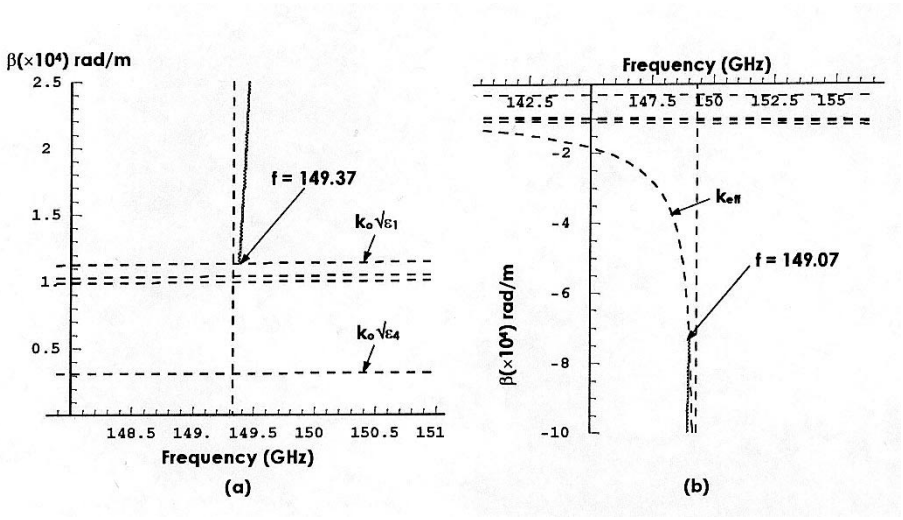

Fig. 10. Enlarged scale of the dispersion diagram $(\beta - f)$. (a) β_{3+} branch. (b) β_{2-} branch.

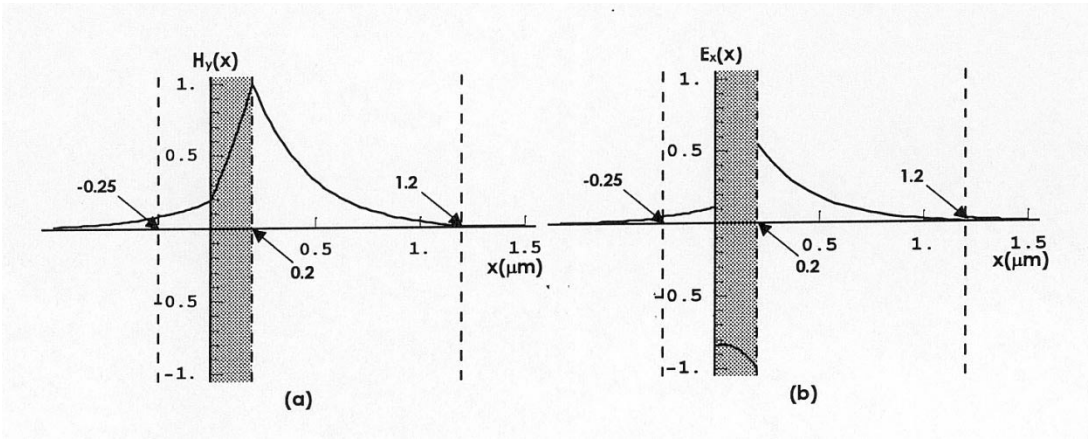

Fig. 11. (a) $H_y(x)$ and (b) $E_x(x)[t=0, z=0]$ for β_{2+} at $f = 140$ GHz in region 2 showing the backward-wave behavior for forward mode. (Field components in normalized units.)

E. Device Considerations

The dispersion diagrams suggest potential device applications for these thin-film structures. For example, in Fig. 3, it can be seen that, over the range $f_{1+} < f < f_{1-}$, only the reverse mode exists and over the range $f_{21+} < f < f_{22+}$, only the forward mode exists. This behavior suggests the possibility of using these two modes for the design of an isolator either over the range f_{1-}–f_{1+} (=27.79 GHz) or over f_{22+}–f_{21+} (=16.3 GHz) provided that the attenuation constant for the single mode of propagation in each case is low. A second possibility for a device based on Fig. 3 is a nonreciprocal phase shifter. For example, at 70 GHz, the differential phase

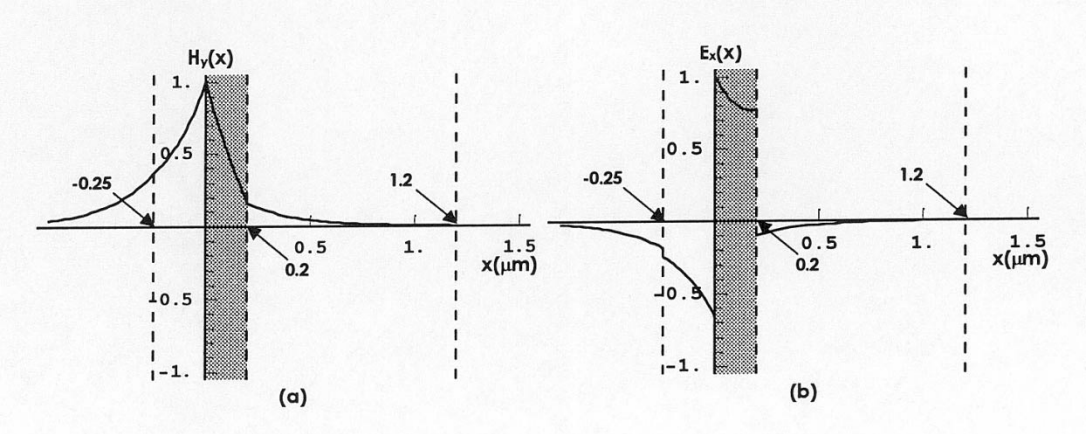

Fig. 12. (a) $H_y(x)$ and (b) $E_x(x)[t = 0, z = 0]$ for β_{2-} at $f = 140$ GHz in region 2 showing the backward-wave behavior for reverse mode. (Field components in normalized units.)

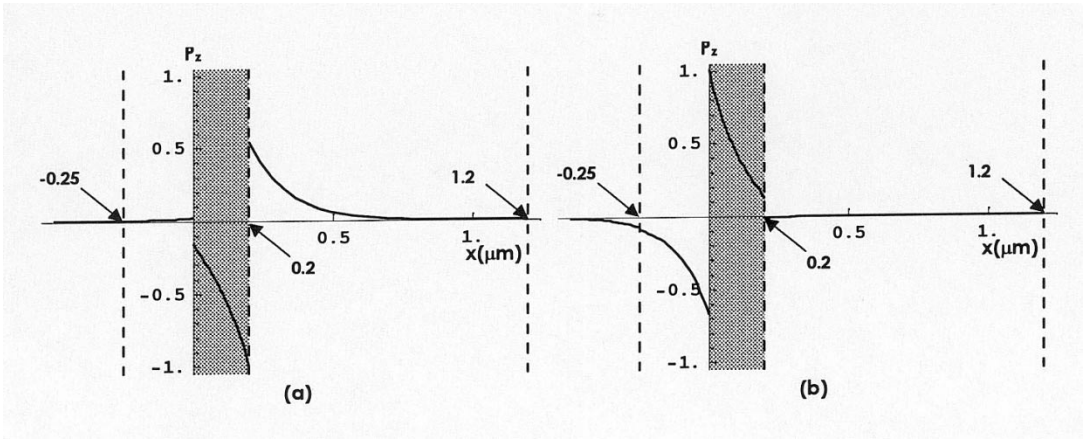

Fig. 13. $P_z = E_x \times H_y$ at $f = 140$ GHz in region 2. (a) β_{2+}. (b) β_{2-}. (Power density in normalized units.)

shift $\Delta\beta = \beta_{1+} - \beta_{1-} = (441.02 - 184.03) \times 10^4$ rad/m $= 2.57$ rad/μm $= 147.25°/\mu$m. Similar comments regarding potential isolators can be made about Fig. 6, but the nonreciprocity between β_{1+} and β_{1-} is slightly larger ($f_{1-} - f_{1+} = 29.63$ GHz) because the asymmetry of the dielectric loading either side of the n-GaAs film is larger. Consequently, at 70 GHz, the (type I) three-film structure in Fig. 6 yields $\Delta\beta = \beta_{1+} - \beta_{1-} = (513.40 - 181.91) \times 10^4$ rad/m $= 3.31$ rad/μm $= 189.65°/\mu$m. In Fig. 9(a) and (b), the nonreciprocal field displacement effect suggests that the (type II) three-film structure in Fig. 7 might be used for a resistive-film field displacement isolator of the type that is familiar in ferrite-loaded waveguides. However, the semiconductor film structure would offer significant miniaturization. For example, the wavelength of magnetoplasmons in each of these structures at 70 GHz is of the order of 1 μm. The statements above provide preliminary guidelines for prospective devices, but the inclusion of losses due to collision mechanisms in the n-GaAs film will require the guidelines to be modified. The real and imaginary parts of ε_{eff} are dependent on ω_p and ω_c, as well as the collision frequency ν_c. With the values of ω_p and ω_c used for the lossless calculations, and assuming $\nu_c = 0.12 \times 10^{12}$ s^{-1}, the two-film waveguide exhibits lowest loss in the frequency range of 60–70 GHz and, in this range, the magnitudes of β_{1+} and β_{1-} are reduced by approximately 50% and 30%, respectively, compared to their lossless values. However, no attempt has been made to optimize the parameters to minimize the loss, and more detailed calculations are in progress.

IV. Conclusion

The nonreciprocal properties of a multilayer n-GaAs-film waveguide on an S-I GaAs substrate with a transverse magnetic field have been explored. The dispersion diagrams and field distributions for three structures each with a total thickness of less than 2 μm have been computed and both forward and backward waves have been found depending on the order in which the films are stacked. Some possibilities for miniature isolators and nonreciprocal phase shifters with lengths of the order of micrometers have been briefly discussed.

Acknowledgment

The authors would like to thank Prof. A. A. Rezazadeh, Dr. J. Sly, and Mr. S. Subramaniam, all of the University of Manchester Institute of Science and Technology (UMIST), Manchester, U.K., for helpful discussions on semiconductor materials. The authors also extend thanks to the reviewers for their constructive comments.

REFERENCES

[1] B. Lax and K. J. Button, *Microwave Ferrites and Ferrimagnetics*. New York: McGraw-Hill, 1962, ch. 12.

[2] J. D. Adam, L. E. Davis, G. F. Dionne, E. F. Schloemann, and S. N. Stitzer, "Ferrite materials and devices," *IEEE Trans. Microwave Theory Tech.*, vol. 50, pp. 721–737, Mar. 2002.

[3] W. L. Bougianni, "Magnetostatic propagation in a dielectric layered structure," *J. Appl. Phys.*, vol. 43, pp. 2541–2548, 1972.

[4] T. J. Gerson and J. S. Nadan, "Surface electromagnetic modes of a ferrite slab," *IEEE Trans. Microwave Theory Tech.*, vol. MTT-22, pp. 757–763, Aug. 1974.

[5] M. S. Sodha and N. C. Srivastava, *Microwave Propagation in Ferrimagnetics*. New York: Plenum, 1981.

[6] D. D. Stancil, *Theory of Magnetostatic Waves*. Berlin, Germany: Springer-Verlag, 1993.

[7] B. S. Yildrim and E.-B. El-Sharawy, "Finite difference time-domain analysis of microwave ferrite devices," in *IEEE MTT-Int. Microwave Symp. Dig.*, vol. 2, 1997, pp. 1113–1116.

[8] S. V. Zagriadski *et al.*, "Electrodynamic theory of multiport structures using magnetostatic waves in ferrite films and its applications," *IEEE Trans. Microwave Theory Tech.*, vol. 51, pp. 744–751, Mar. 2003.

[9] A. S. Akyol and L. E. Davis, "A novel nonreciprocal ferrite image guide," in *IEEE MTT-S Int. Microwave Symp. Dig.*, vol. 2, 2001, pp. 1179–1182.

[10] ——, "Measurements of a leaky wave ferrite isolator," *IEEE Trans. Microwave Theory Tech.*, vol. 51, pp. 1476–1481, May 2003.

[11] R. E. Collin, *Field Theory of Guided Waves*. New York: IEEE Press, 1991, ch. 11.

[12] P. Yeh, *Optical Waves in Layered Media*. New York: Wiley, 1988.

[13] K. W. Chiu and J. J. Quinn, "Magnetoplasma surface waves in polar semiconductor: Retardation effects," *Phys. Rev. Lett.*, vol. 29, no. 9, pp. 600–603, Aug. 1972.

[14] J. J. Brion and R. F. Wallis, "Theory of surface magnetoplasmons in semiconductors," *Phys. Rev. Lett.*, vol. 28, no. 22, pp. 1455–1458, May 1972.

[15] N. Marschall and B. Fischer, "Dispersion of surface polaritons in GaP," *Phys. Rev. Lett.*, vol. 28, no. 13, pp. 811–813, Mar. 1972.

[16] A. Hartstein and E. Burstein, "Observation of magnetoplasma type surface polaritons on n-type InSb," *Solid State Commun.*, vol. 14, pp. 1223–1227, 1974.

[17] R. F. Wallis, J. J. Brion, E. Burstein, and A. Hartstein, "Theory of surface polaritons in anisotropic dielectric media with application to magnetoplasmons in semiconductors," *Phys. Rev. B, Condens. Matter*, vol. 9, no. 8, pp. 3424–3437, Apr. 1974.

[18] M. S. Kushwaha and P. Halevi, "Splitting of surface polaritons dispersion curves due to resonance with magnetoplasma transition layer," *Solid State Commun.*, vol. 64, no. 11, pp. 1405–1408, 1987.

[19] R. E. Hayes and W. G. May, "The use of semiconductors in nonreciprocal devices for submillimeter wavelengths," in *Proc. Submillimeter Waves Symp.*, Brooklyn, NY, 1970, pp. 237–250.

[20] M. Kanda and W. G. May, "Nonreciprocal reflection-beam isolators for far-infrared use," *IEEE Trans. Microwave Theory Tech.*, vol. MTT-21, pp. 786–790, Dec. 1973.

[21] ——, "Hollow-cylinder waveguide isolators for use at millimeter wavelengths," *IEEE Trans. Microwave Theory Tech.*, vol. MTT-22, pp. 913–917, Nov. 1974.

[22] D. M. Bolle and S. H. Talisa, "Fundamental considerations in millimeter and near-millimeter component design employing magnetoplasmons," *IEEE Trans. Microwave Theory Tech.*, vol. MTT-29, pp. 916–923, Sept. 1981.

[23] V. H. Mok and L. E. Davis, "Nonreciprocal GaAs phase-shifters and isolators for millimetric and sub-millimetric wavelengths," in *IEEE MTT-S Int. Microwave Symp.*, vol. 3, June 2003, pp. 2249–2252.

[24] M. R. Brozel and G. E. Stillman, *Properties of Gallium Arsenide*, 3rd ed, London, U.K.: INSPEC–IEE, 1996.

[25] B. Lax, "Magnetoplasma effects in solids," *IRE Trans. Microwave Theory Tech.*, vol. MTT-9, pp. 83–89, Jan. 1961.

[26] R. Sloan and L. E. Davis, "Broad-band theoretical gyroelectric junction circulator tracking behavior at 77 K," *IEEE Trans. Microwave Theory Tech.*, vol. 44, pp. 2655–2660, Dec. 1996.

[27] C. K. Yong, R. Sloan, and L. E. Davis, "A Ka-band indium–antimonide junction circulator," *IEEE Trans. Microwave Theory Tech.*, vol. 49, pp. 1101–1106, June 2001.

[28] S. M. Sze, *Physics of Semiconductor Devices*, 2nd ed. New York: Wiley, 1981.

[29] R. People and J. C. Bean, "Calculation of critical layer thickness versus lattice mismatch for Ge_xSi_{1-x}/Si strained-layer heterostructures," *Appl. Phys. Lett.*, vol. 47, no. 3, pp. 322–324, Aug. 1985.

[30] S. H. Wei and A. Zunger, "Optical properties of zinc–blende semiconductor alloys: Effects of epitaxial strain and atomic ordering," *Phys. Rev. B, Condens. Matter*, vol. 49, no. 20, pp. 14337–14351, May 1994.

[31] S. Jain, M. Wilander, and R. V. Overstraeten, *Compound Semiconductors Strained Layers and Devices*. Boston, MA: Kluwer, 2000.

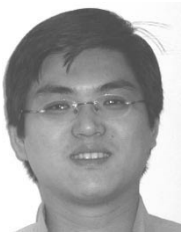

Vee H. Mok (S'99–M'01) was born in Perak, Malaysia, on October 20, 1972. He received the B.Eng. (Hons.) degree in electrical and electronic engineering (with first-class honors) from the University of Manchester Institute of Science and Technology (UMIST), Manchester, U.K., in 2000.

His research interests are nonreciprocal microwave devices using semiconductor material and negative refractive index materials.

Mr. Mok is the chairman and founder of the UMIST IEEE Student Branch. He is also a member of the Institution of Electrical Engineers (IEE), U.K. He was the recipient of a British Overseas Research Scholarship (ORS), a UMIST Graduate Research Scholarship (GRS), and a Microwave Research Scholarship for his doctoral studies in microwave engineering.

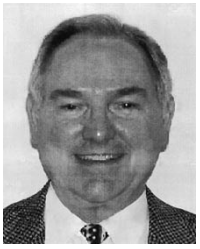

Lionel E. Davis (SM'64–LF'95) received the B.Sc. (Eng.) degree from the University of Nottingham, Nottingham, U.K., and the Ph.D. and D.Sc. (Eng.) degrees from University College London, London, U.K.

From 1959 to 1964, he was with Mullard Research Laboratories, Redhill, U.K. From 1964 to 1972, he was a faculty member with the Electrical Engineering Department, Rice University, Houston, TX. From 1972 to 1987, he was with Paisley College, Paisley, Scotland, where he was Professor and Head of the Department of Electrical and Electronic Engineering. In 1987, he joined the Department of Electrical Engineering and Electronics, University of Manchester Institute of Science and Technology (UMIST), Manchester, U.K., where he is currently Professor of communication engineering and Head of the Microwave Engineering Group. He has been a Visiting Professor with the University College London and the University of California at San Diego, and has been a consultant for several companies. He has carried out research on passive components, high-T_c superconductors, dielectric-resonator antennas, chiral materials, and liquid crystal films. His current research interests are in gyrotropic media and nonreciprocal components for microwave, millimeter-wave, and optical wavelengths.

Dr. Davis is a Fellow of the Institution of Electrical Engineers (IEE), U.K., and of the Institute of Physics. He is a member of the IEEE Microwave Theory and Techniques Society (IEEE MTT-S) International Microwave Symposium (IMS) Technical Programme Committee, and co-chairman of the IEEE MTT-S Committee on Microwave Ferrites. Until recently, he was a member of the Administrative Committee of the UKRI MTT/AP/ED/LEOS chapter, and he initiated the Houston chapter of the IEEE MTT-S. He served on the Council, the Microwave Theory and Devices Committee, and the Accreditation Committee of the IEE and is a member of the Peer Review College of the U.K. Engineering and Physical Sciences Research Council (EPSRC).